Supporting Information

Passivation-Driven Speciation, Dealloying and Purification

*Andrew Martin,[1] Boyce Chang,[1] Joel Cutinho,[1] Liyang Shen,[2] Thomas Ward III,[3] Eric W. Cochran,[2] Martin M. Thuo[1,4,5,]**

[1]Department of Materials Science and Engineering, Iowa State University, Ames, IA-50010. USA
[2]Department of Chemical and Biological Engineering, Iowa State University, Ames, IA-50010. USA
[3]Department of Aerospace Engineering, Iowa State University, Ames, IA-50010. USA
[4]Micro-Electronics Research Center. Ames, IA-50010. USA
[5]Department of Electrical and Computer Engineering, Iowa State University. Ames, IA-50010. USA

Experimental Section

Materials: Field's metal (32.5% Bi, 51% In, 16.5% Sn, T_m = 355 K), Bi-Sn alloy (58% Bi, 42% Sn, T_m = 411 K) and In-Sn alloy (52% In, 48% Sn, T_m = 391 K) were purchased from Rotometals inc. Diethylene glycol (99%) was purchased from Alfa Aesar. Ethyl acetate (99.9%), glacial acetic acid (99.7%), trichloroacetic acid (99.8%) was purchased from Fisher Chemical.

Undercooled Liquid Metal Core-Shell Particle Synthesis: Undercooled core-shell metal particles were synthesized using shearing into complex particles (SLICE) method, a previously reported procedure.[1] Detailed procedure of this mechanism is included in the SI.

SEM Characterization: Metal particles stored in ethyl acetate solution were transferred onto silicon wafer using pipettes and then were characterized by Scanning Electron Microscopy (FEI Quanta 250 FEI-SEM). Samples are mounted on standard SEM mount (Ted Pella Inc.) adhered with copper tape. The SEM was operated under high vacuum at a voltage of 10-15 kV with spot size of 3 at 10 mm working distance. Everhart-Thorley Secondary electron detector and backscatter detector were used to take micrographs at various magnifications. Size measurements for features were done using ImageJ software

Focused Ion Beam (FIB)-SEM Analysis: The sample was prepared using a FEI Helios NanoLab G3, on a 38-degree back-tilt holder with the sample attached to the back-tilted portion of the

stub. Initial machining was carried out at 4 mm working distance (eucentric height) at 30kV on the Ion column, with a 5kV finishing step, the machining was performed at zero-tilt, so that the machined surface was 52-degrees with respect to the electron column axis.

TGA Heat Treatment: The particles were heat treated using Thermogravimetric Analyzer (Q50 TGA, TA Instruments). The particles were then drop casted onto undoped silicon wafers that are previously cleaned using ethanol and dried with ultrahigh-purity nitrogen gas. Sample was then placed on a platinum TGA pan. The heat treatment was carried in presence of air, with helium purge gas. Purge gas flow rate was set at 60ml/min and heating ramp rate at 10°C/min up to 1000°C.

Thermogravimetric Analysis (TGA)-Infrared (IR)-Mass Spectrometry (MS) Analysis: Coupled TGA-IR-MS instrument (Netzsch STA449F1) was used to analyze mass change and evolved gas released during particle's heat treatment. Sample was deposited and dried in an alumina crucible with a matching reference crucible used. Simulated dry air (80% oxygen 20% nitrogen) was used as the purge gas. Sample was then loaded and ran through a heating ramp step at 10°C/min. Obtained raw data was analyzed using Proteus and Opus software.

High-Temperature X-Ray Diffraction (HTXRD) Analysis: Panalytical (PW3050/60) XRD with Co tube and Panalytical X'celerator detector was used to analyze changes in x-ray diffraction whith heated in-situ. Heated non-ambient chamber (Malvern HTK-1200N) inside the instrument. Co tube with Fe filter at 0.04 soller rad slit was used. All experiments were done at 0.02° step size with 60s/step rate.

Small Angle X-Ray Scattering (SAXS) Analysis: The SAXS measurements were performed at the Xenocs Xeuss 2.0 UHR system. The Field's metal particles were placed between Kapton tapes in washers and then put in a sample holder inside the measurement chamber. The source was copper with radiation wavelength 0.154 nm. All the SAXS measurements were carried out at room temperature under vacuum.

Particle Synthesis

Field's Metal SLICE: Materials used include Field's metal, glacial acetic acid, ethyl acetate and diethylene glycol. 20 g of Field's metal was deposited in 1 vol% acetic acid – diethylene glycol solution (~200 g) and heated up to 120°C in a glass beaker of the soup maker (Cusinart SBC-1000FR). After thermal equilibrium reached in 5-7 min, the solution was sheared on a ~10^{o} angle for 4 min at about 17,000 rpm. Excess acetic acid-diethylene glycol solution was washed out with ethanol using Whatman GF/F filter using a Buchner filter and particles were stored in ethyl acetate solution after cleaning.

BiSn SLICE: Materials used include eutectic BiSn metal, trichloroacetic acid, ethyl acetate and diethylene glycol. 10 g of BiSn was deposited in 1 vol% trichloroacetic acid – diethylene glycol solution (~200 g) and heated up to 170°C in a glass beaker. The solution was equilibrated at said temperature and then transferred to a preheated soup maker, wrapped in heating tape and aramid blanket (Cusinart SBC-1000FR). The solution was sheared on a ~10^{o} angle for 4 min at about 17,000 rpm. Excess trichloroacetic acid-diethylene glycol solution was washed out with ethanol using Whatman GF/F filter using a Buchner filter and particles were stored in ethyl acetate solution after cleaning.

InSn SLICE: Materials used include InSn metal, glacial acetic acid, ethyl acetate and diethylene glycol. 10 g of InSn was deposited in 1 vol% acetic acid – diethylene glycol solution (~200 g) and heated up to 150°C in a glass beaker. The solution was equilibrated at said temperature and then transferred to a preheated soup maker, wrapped in heating tape and aramid blanket (Cusinart SBC-1000FR). The solution was sheared on a ~10^{o} angle for 4 min at about 17,000 rpm. Excess acetic acid-diethylene glycol solution was washed out with ethanol using Whatman GF/F filter using a Buchner filter and particles were stored in ethyl acetate solution after cleaning.

Calculation on Volumetric Change due to Phase Transition

Volumetric changes during phase transition was calculated using values in table S1. Assuming 1g of starting material, volumes of each elements were calculated in proportion for each alloy. ΔV for each element can then be calculated by taking V_{sol}-V_{liq}. Based on whether the material is contracting or expanding upon solidification, Contraction vs. expansion ratio ($\Delta V_{contract}/\Delta V_{expand}$) can be calculated to measure the amount of stress exerted during phase transition.

For example, 1g of Field's metal contain 0.51 g In, 0.325 g Bi and 0.165 g Sn. ΔV_{In} after liquid-solid phase transition is -2.8 mm^3, whilst ΔV_{Sn} = -1.03 and ΔV_{Bi} = 0.90. Taking a total of the contracting elements (In and Sn) and dividing it with the expanding element (Bi). Gives us the contraction-expansion ratio of 4.34. Same concept can be applied to BiSn to where it yields a ratio of 1.83. No ratio is found for InSn due to the lack of expanding element.

Table S1. Material properties for elements forming the alloys used in this work.[2-5]

Element	Density (g/cm^3)	Elastic Modulus (GPa)	Thermal Expansion Coeff. ($\cdot 10^{-6}$ K^{-1})	E^0 (V)
Indium (S)	7.02	10	33	-0.338
Indium (L)	7.31			
Bismuth (S)	9.78	32	13.2	0.317
Bismuth (L)	10.022			
Tin (S)	7.31	50	22	-0.14
Tin (L)	6.99			

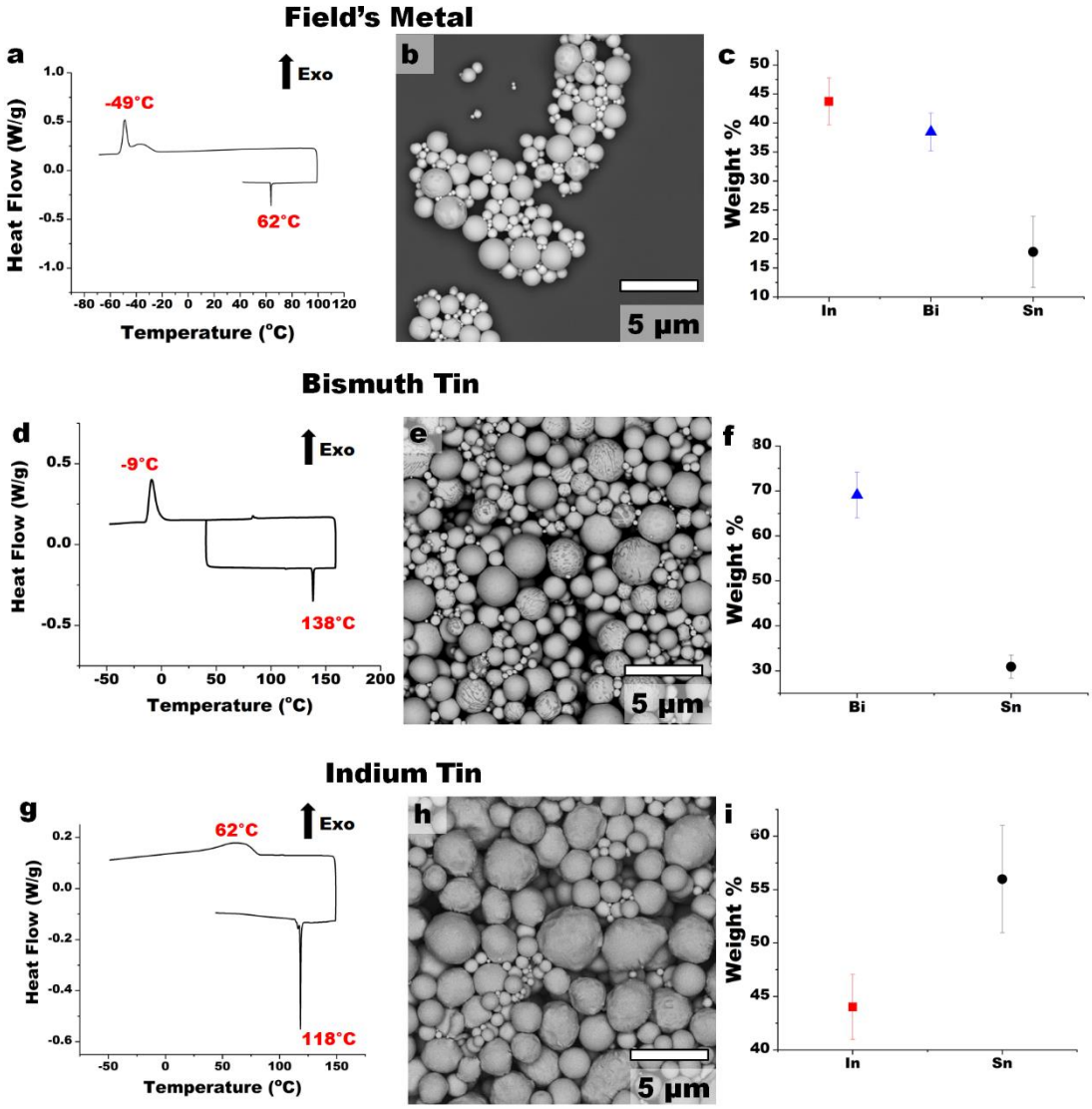

Figure S1. DSC Trace, SEM and EDS analysis of synthesized (a-c) Field's metal particles, (d-f) eutectic bismuth-tin particles and (g-i) eutectic indium-tin particles.

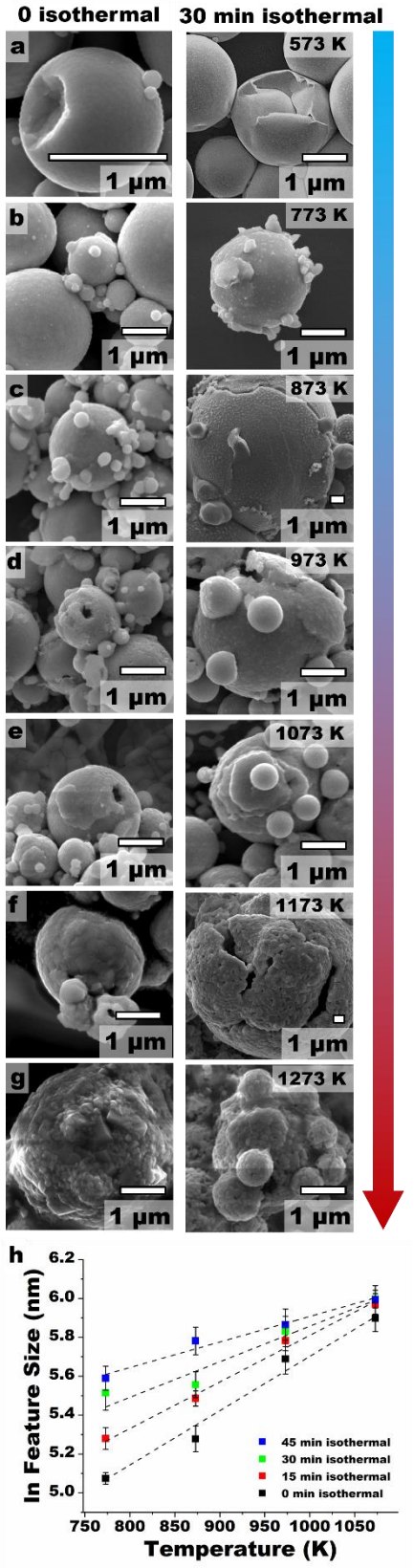

Figure S2. SEM Micrographs of heat-treated Field's metal particles with 0 and 30 minutes isothermal time at (a) 573 K, (b) 773 K, (c) 873 K, (d) 973 K, (e) 1073 K, (f) 1173 K, (g) 1273 K. (h) Changes in grown feature sizes with changes in temperature and isothermal time.

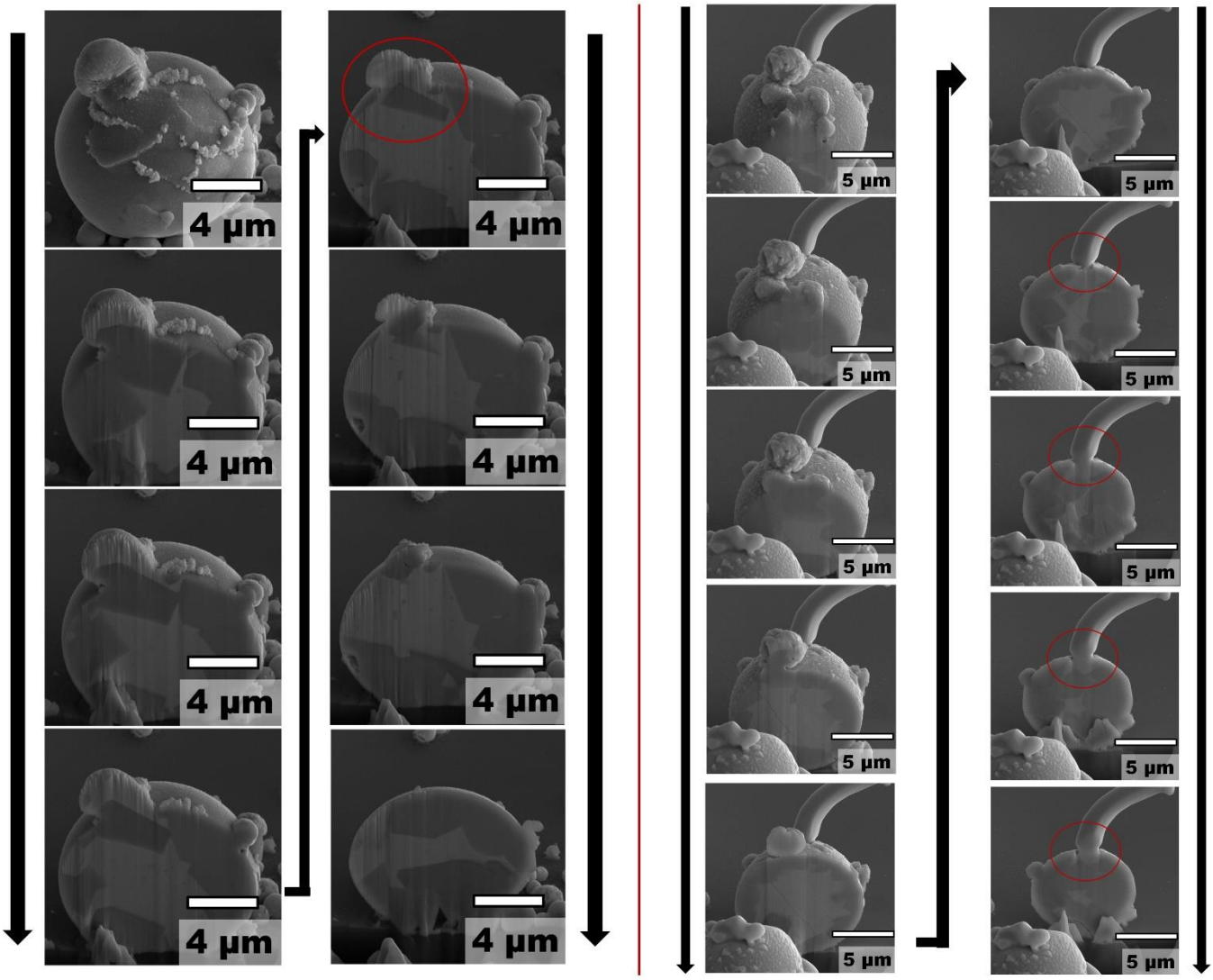

Figure S3. Periodic FIB-SEM cross section of heat-treated Field's metal particles at 873 K with 30 minutes isothermal time.

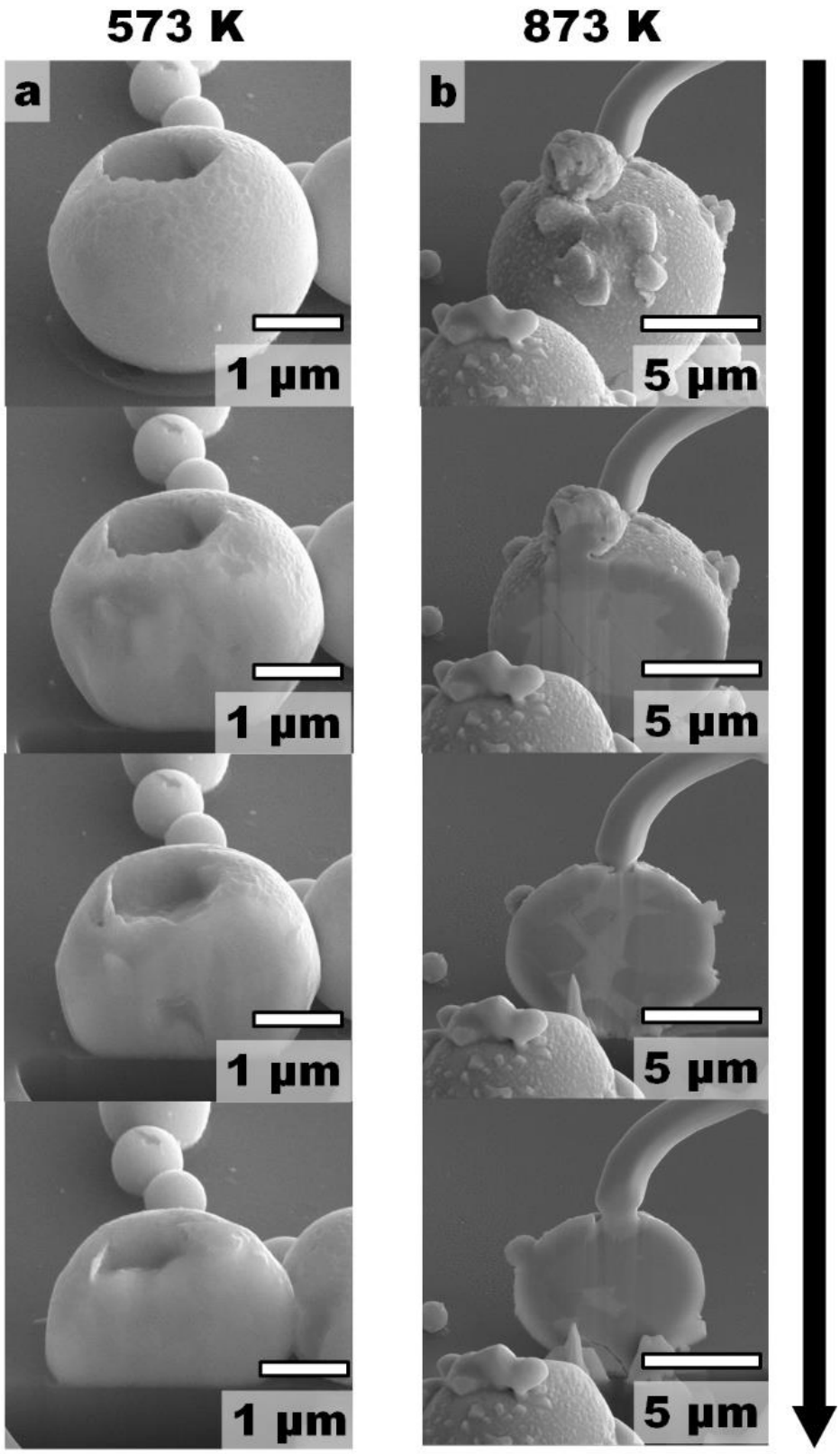

Figure S4. Periodic FIB-SEM cross section of heat-treated Field's metal particles at (a) 573 K and (b) 873 K.

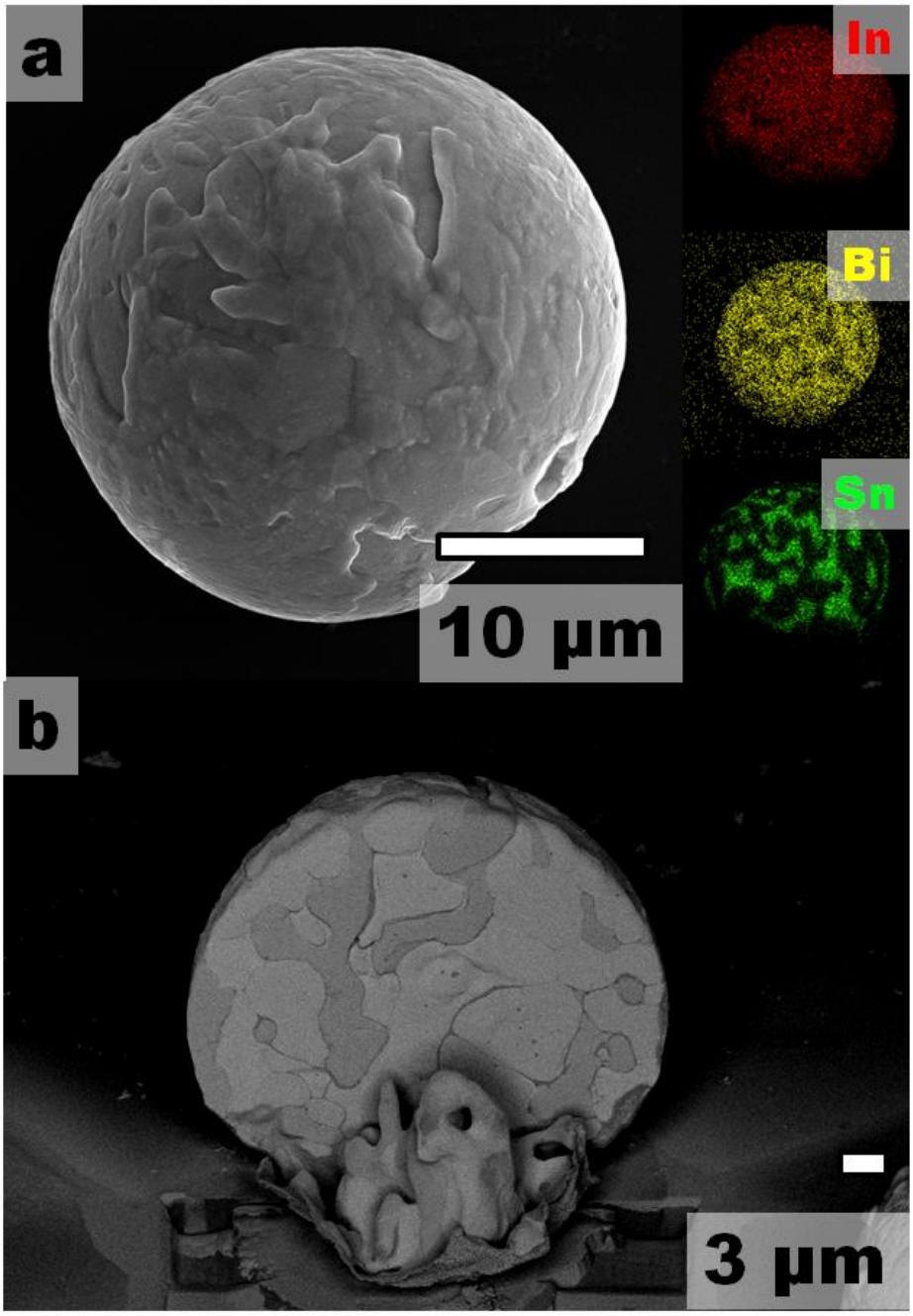

Figure S5. (a) EDS map of solid Field's metal particles synthesized with SLICE (b) FIB-SEM cross section of particle shown in a.

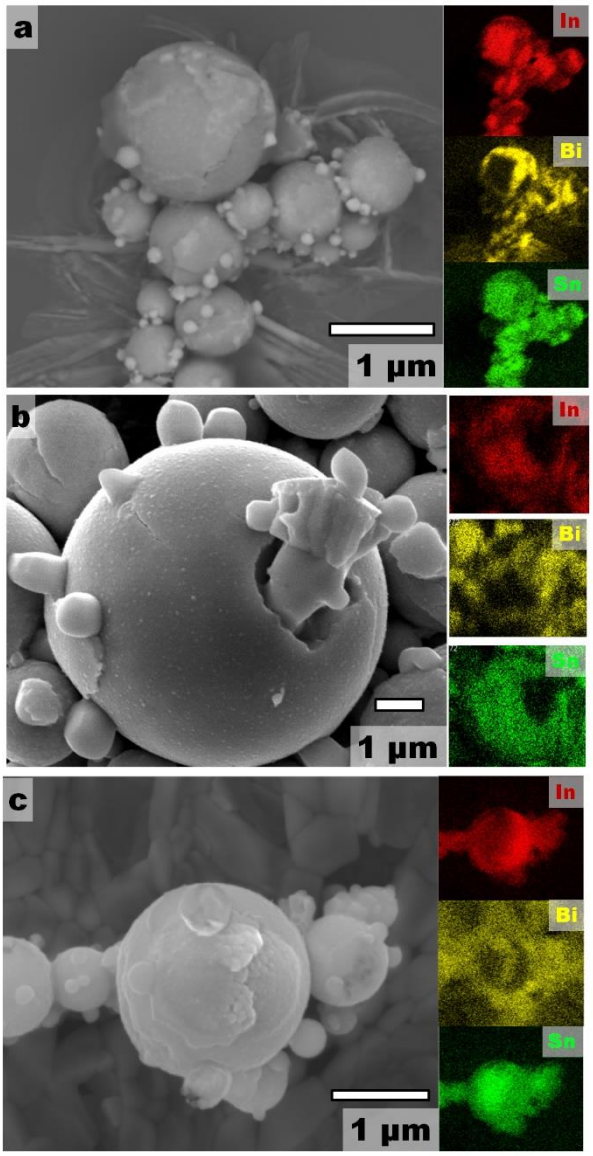

Figure S6. EDS map of heat-treated Field's metal particles at (a) 773 K 0 isothermal time, (b) 873 K 30 minutes isothermal time, and (c) 973 K 0 isothermal time.

SAXS Dimensional analysis background

The existence of a diffuse boundary is observed where there is a negative deviation from the ideal Porod's law constant (α = 4) on the slope of the scattering intensity (Figure 3c).[6] The scattering vector q in these plots relates the scattering angle and the wavelength of the radiation used in this experiment ($q = 4\pi sin\theta/\lambda$), where θ is half the scattering angle and λ is the wavelength. The amount of deviation from the ideal exponent indicates that the electron density profile is not sharp, larger deviation can be suspected of thicker oxides. It can be seen that α increases as the particles are heated to 523 K (from -4.33 to -4.64), which indicates a growing

oxide shell. The deviation, however, decreases as the particles reaches 773 K and even further to 1023 K, almost reaching the ideal value. We suspect that at 773 K, the oxide has reached a critical thickness to which it is no longer diffuse. This temperature also marks the emergence of the bismuth features (figure 2b), which suggests that fracturing already occurs, meaning the oxides already lose plasticity. As the particles are continually heated, these features will grow larger as the oxide also grows thicker (figure S5c). At this point, the oxides would have formed larger crystalline structures that would no longer have a diffuse boundary with the bulk metal and thus the deviation disappears. Ruland's method was used to approximate the boundary thickness (figure S7c), the plot was created based on the relationship: $I(q) = K_p \cdot q^{-4} e^{(-\sigma^2 q^2)}$, where σ (the slope in this plot) is the standard deviation of a gaussian smoothing function and K_p is the Porod's law constant, thickness of the oxide (t) can be calculated using the relationship: $t = \sqrt{2\pi\sigma}$. From figure 3d. it can be approximated that the fresh oxide of the ULMCS is about ~7.3 nm and it can grow up to ~9.6 nm at 523 K. At 773 K and beyond, the plot displays a straight horizontal line, which gives no approximation of oxide thickness. With this information, it is safe to assume that the oxide will continually grow while heated, upon reaching a critical point, the oxide will undergo crystallization and form the large features shown in figure 2.

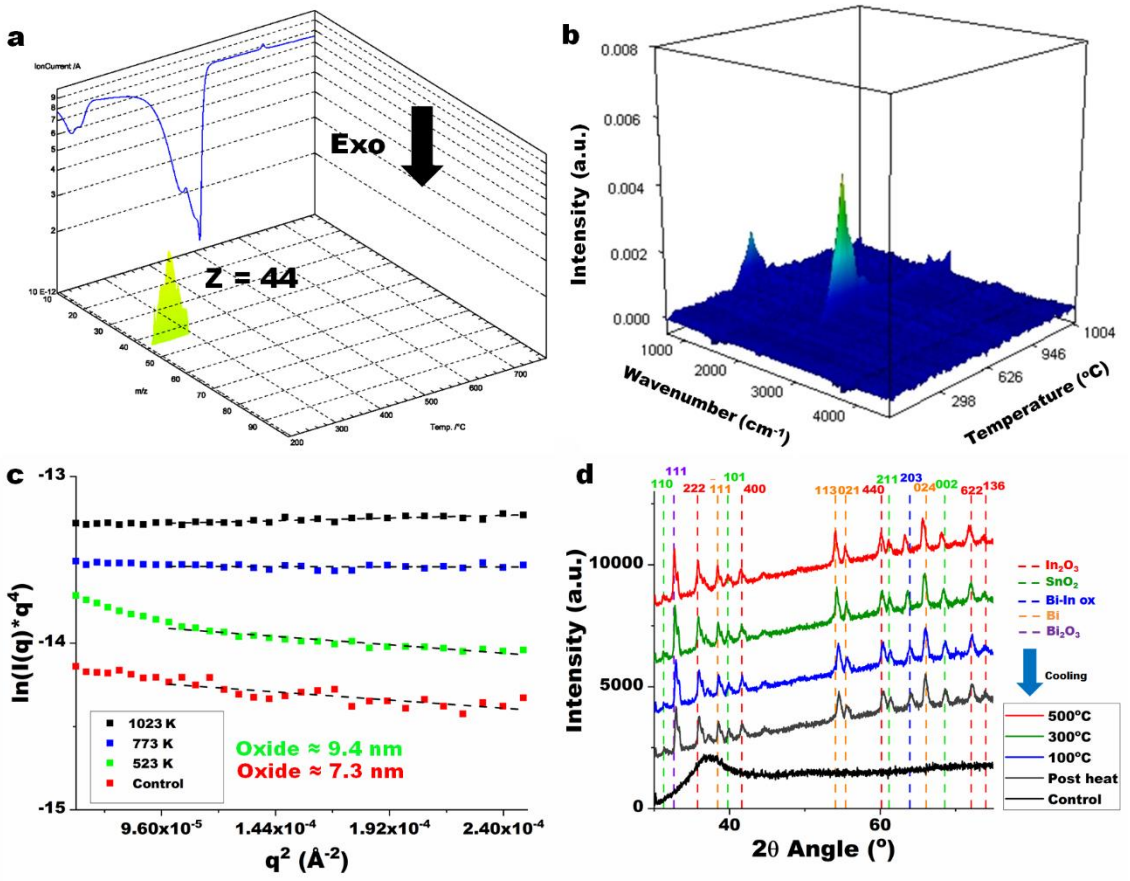

Figure S7. (a) Mass Spectroscopy and (b) IR spectroscopy of heated FM particles. (c) Ruland's method calculation with SAXS dimensional analysis (d) Full HTXRD curves for heat-treated Field's metal particles.

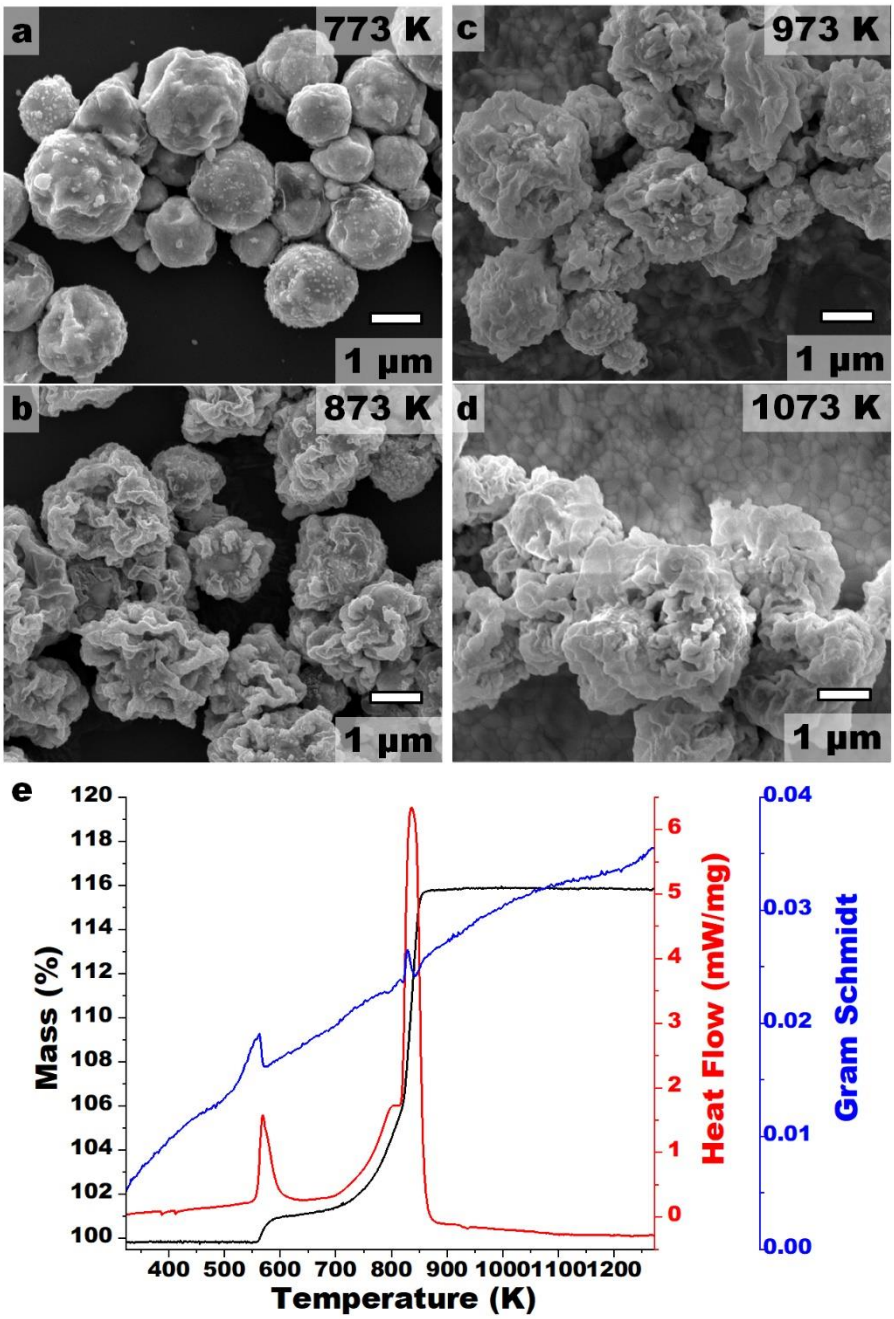

Figure S8. SEM Micrographs of heat-treated bismuth-tin metal particles with 0 minutes isothermal time at (a) 773 K, (b) 873 K, (c) 973 K and (d) 1073 K. (e) DSC-TGA-Gram Schmidt of heat treated BiSn particles.

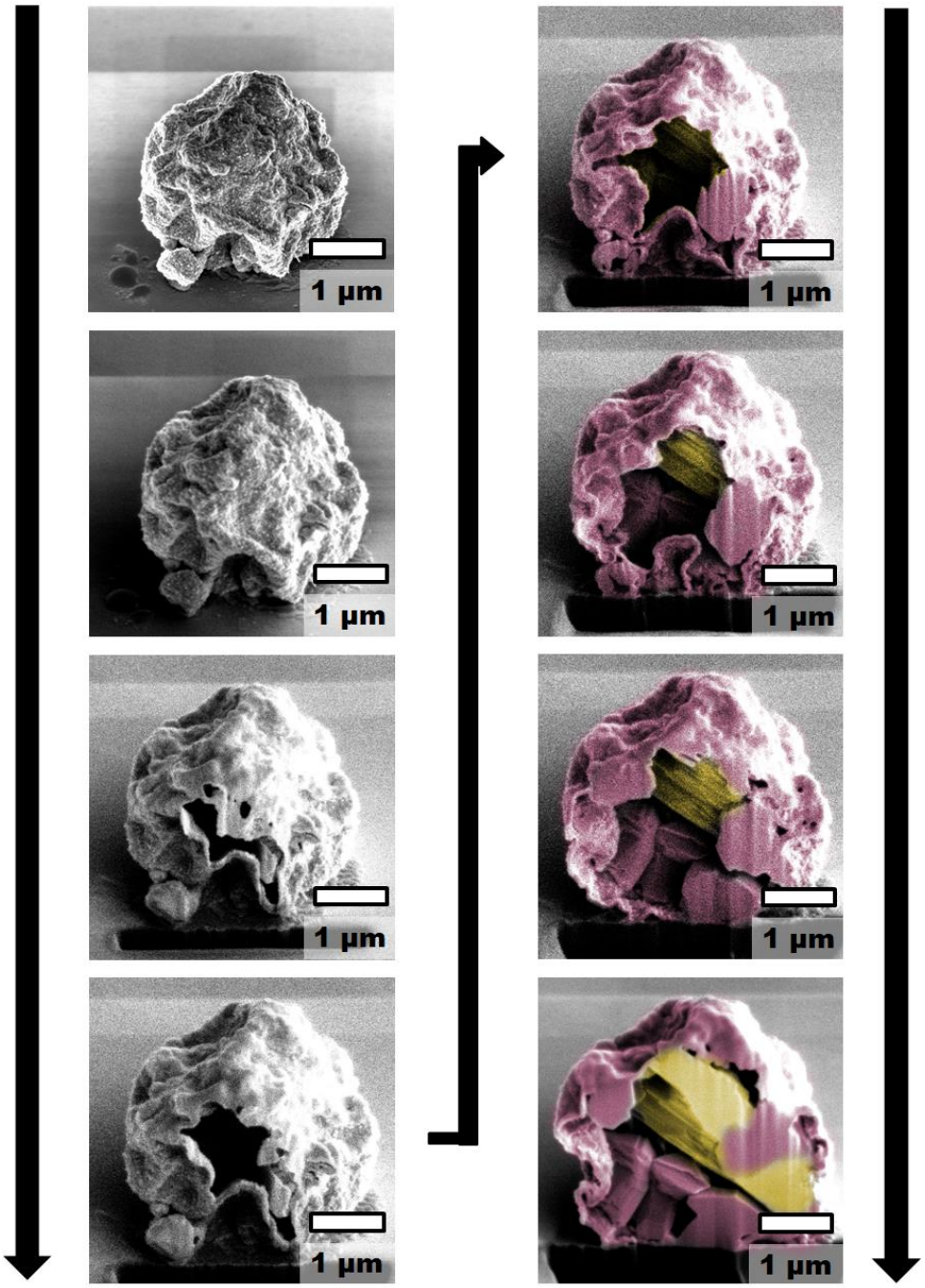

Figure S9. Periodic FIB-SEM cross section of heat-treated BiSn particles at 873 K with 0 minutes isothermal time.

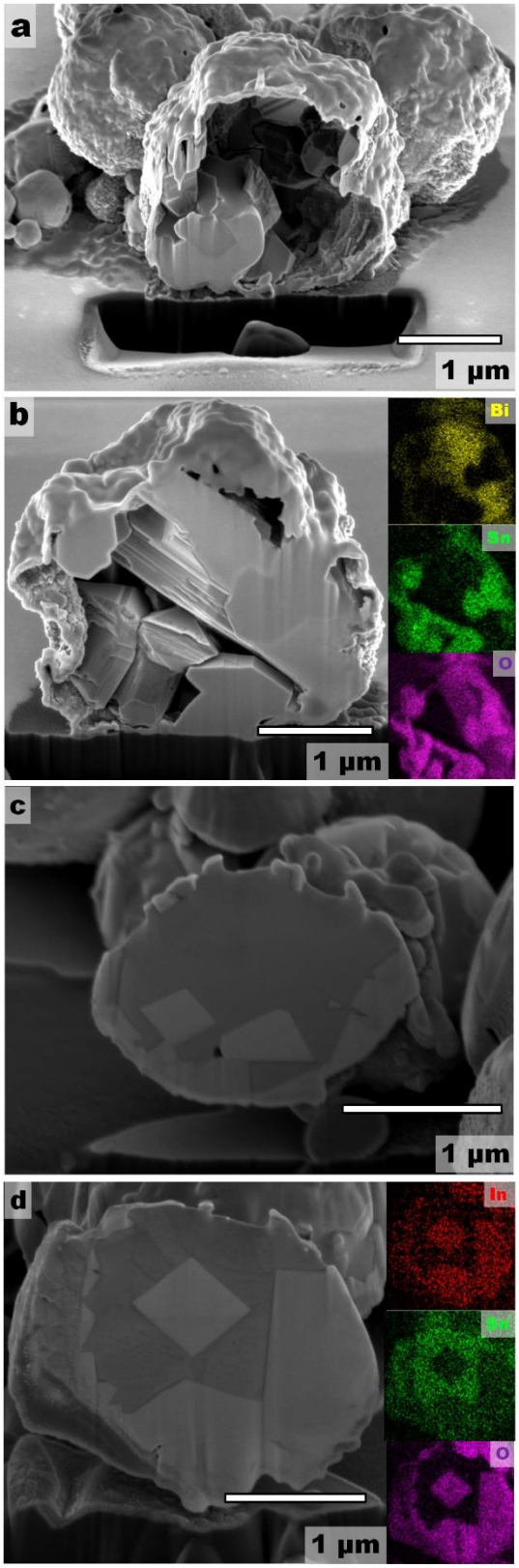

Figure S10. (a-b) FIB-SEM and EDS from cross section of heat-treated BiSn particles at 873 K. (c-d) FIB-SEM and EDS from cross section of heat-treated InSn particles at 873 K.

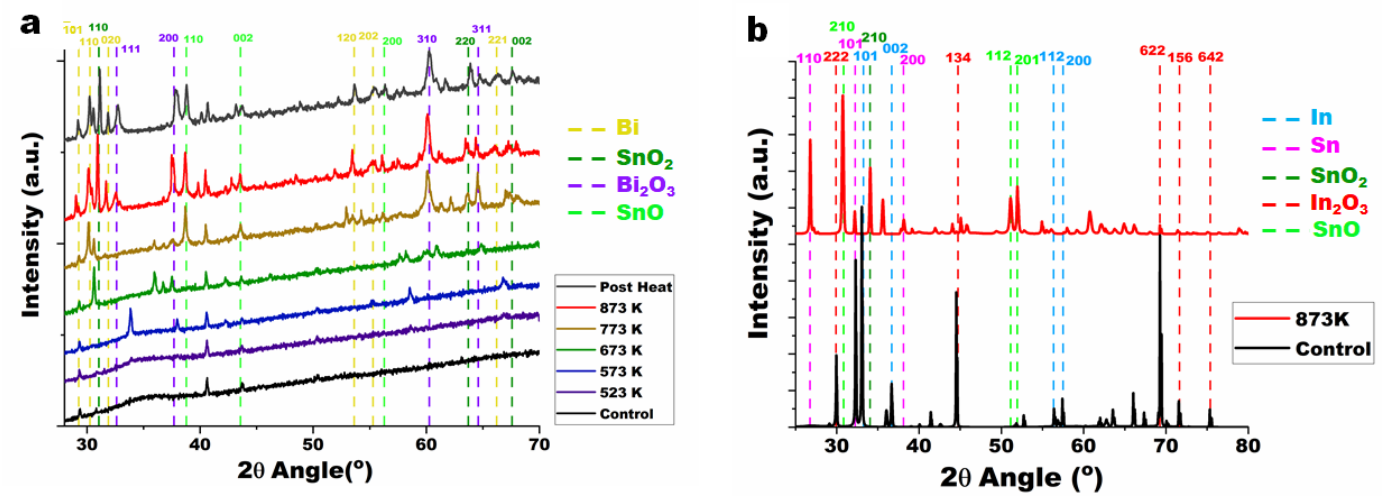

Figure S11. (a) in-situ HTXRD analysis on BiSn particles. (b) XRD of InSn particles before and post heating.

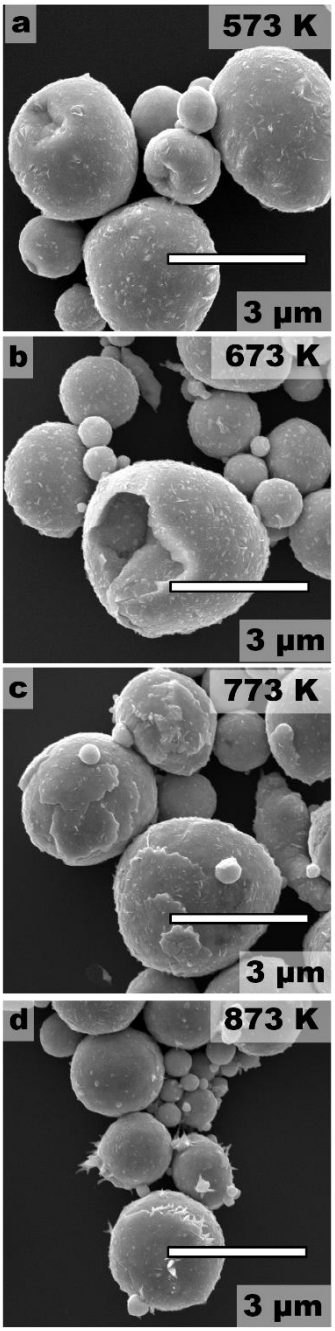

Figure S12. SEM Micrographs of heat-treated indium-tin metal particles with 0 minutes isothermal time at (a) 573 K, (b) 673 K, (c) 773 K and (d) 873 K.

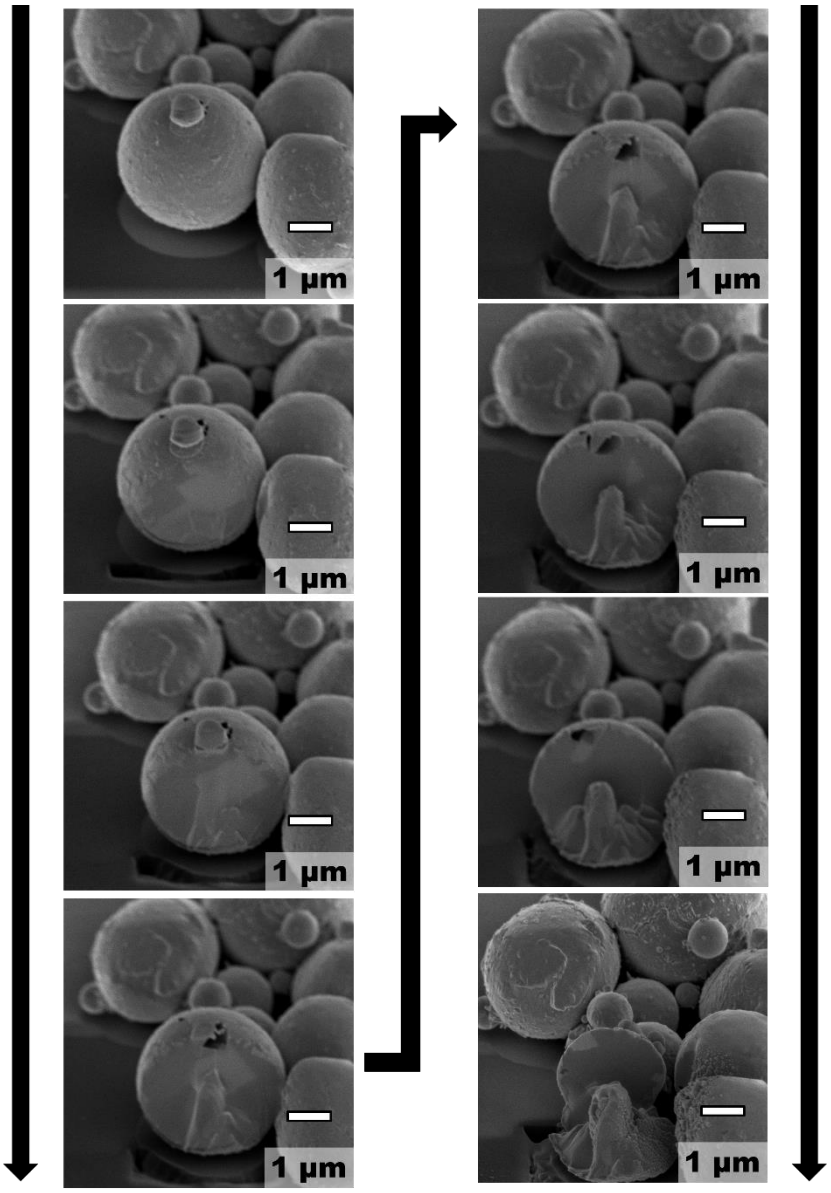

Figure S13. Periodic FIB-SEM cross section of heat-treated InSn particles at 873 K with 0 minutes isothermal time.

References:

1. I. D. Tevis, L. B. Newcomb and M. Thuo, *Langmuir*, 2014, **30**, 14308-14313.
2. E. Cave and L. Holroyd, *J. Appl. Phys.*, 1960, **31**, 1357-1358.
3. J. Smith and V. Schneider, *J. Less Common Met.*, 1964, **7**, 17-22.
4. J. Thewlis and A. Davey, *Nature*, 1954, **174**, 1011-1011.
5. V. Deshpande and D. Sirdeshmukh, *Acta Cryst.*, 1961, **14**, 355-356.
6. G. Porod, *Kolloid-Z*, 1951, **124**, 83-114.